Optical Properties of Ag and α-Phase Ag-Al Alloys*

G. B. Irani,† T. Huen, and F. Wooten
Lawrence Radiation Laboratory and Department of Applied Science, University of California, Livermore, California 94550
(Received 15 October 1970)

Reflectance measurements at nearly normal incidence were used to investigate the optical properties and electronic band structure of Ag and dilute alloys of Al in Ag. Sample films were prepared, maintained, and measured in ultrahigh vacuum with base pressures less than 10^{-9} Torr. Measurements were made in the spectral range 1.1–11.5 eV. Shifts in the ϵ_2 peak at 4.54 eV ($L_3 \rightarrow L_{2'}$) are at one-half the rate expected for the rigid-band model. The implication is that the shielding cloud around the Al impurities saturates the band allowance of two electrons per atom. The weak $L_2 \rightarrow L_1$ transition, hidden under the $L_3 - L_{2'}$ transition in pure Ag, shifts to lower energy in the alloys. The transition with ϵ_2 peak at 5.73 eV is not shifted by alloying.

I. INTRODUCTION

This paper is concerned with the optical properties of α-phase alloys of aluminum in silver. The aim of the work reported here was to gain some insight into the applicability of different models of alloys.[1-4]

A number of characteristics recommend the α-phase Ag-Al alloys for study. Aluminum has the same crystal structure (fcc) and very nearly the same lattice spacing and atomic radius as silver. Thus, when silver atoms are replaced by aluminum atoms, little distortion of the lattice occurs, and change in the free energy of the alloy depends largely on electronic levels. Aluminum has no *d* states of its own to contribute to the valence band of the alloy. It acts largely just to shift and broaden structure related to the silver matrix. It is the direction of shift in structure that aids in correlating optical transitions with electronic band-structure calculations. The magnitude of shifts in transitions to or from the Fermi surface serves as a check on the validity of, e.g., the rigid-band model[1] or Friedel's model of dilute alloys.[2]

II. EXPERIMENTAL

A. Reflectometer

A sketch of the reflectometer is shown in Fig. 1. Design details are discussed elsewhere.[5] Only a brief description is presented here.

As shown in Fig. 1, the reflectometer system has two chambers. The sample is prepared in the upper chamber and then moved linearly downward into the reflectance chamber. Monochromatic light enters this chamber through a LiF window. When in operation, the ellipsoidal mirror rotates at 1200 rpm and the angular speed is precisely regulated. The rotation causes the incident and reflected sample beam intensities to be detected alternately in time. The result is a series of current pulses from the photomultiplier tube (detector). This is illustrated in Fig. 2. The reflectance ratio is then electronically computed with the aid of the electronic system shown schematically in Fig. 3. The desired spectral reflectance curve is obtained by recording the ratio as the wavelength is slowly, but automatically, scanned.

An important feature of the reflectometer, not shown in Fig. 1, is a stainless-steel can that surrounds the filaments. The can contains a plate which prevents evaporated material from one filament from reaching the other; it restricts the evaporation from each filament to a (1.6×2.2) cm^2

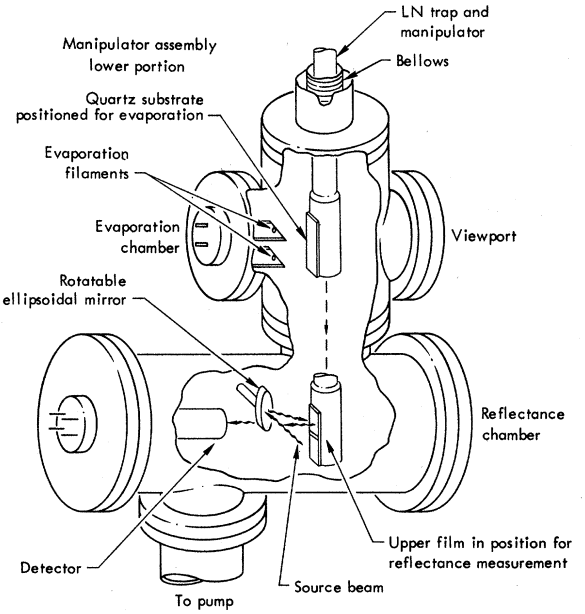

FIG. 1. Reflectometer, as viewed from the monochromator.

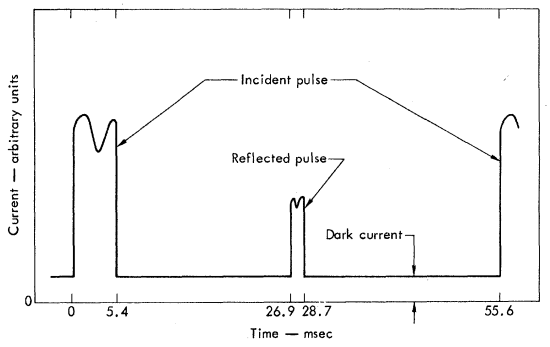

FIG. 2. Reflectance signal. Sketch shows current pulses from the photomultiplier tube. Pulse shapes indicate the variation of sensitivity as beam sweeps across the photocathode. Dark current displacing the pulses above zero is exaggerated for clarity. The reflected pulse duration is one-third of the incident pulse duration.

area of the substrate, and it holds two extra substrates for each filament. The role of the extra substrates is discussed in Sec. II B.

The manipulator is a hollow stainless-steel pipe with a copper bottom. It serves to lower the sample into position after the sample is prepared in the upper chamber. It also provides a thermal path to the sample via the copper bottom. After the sample films have been prepared, they can be annealed by inserting a heating rod down into the manipulator.

B. Sample Preparation

Alloys were prepared in a graphite crucible from high-purity constituents (99.999%) in a demountable vacuum system which provided rf induction heating and a base pressure less than 10^{-6} Torr. The graphite crucible provided two essential properties: It coupled well with the rf field and was immiscible with Ag and the Ag-Al alloys. Pure Al did adhere to the crucible, but this problem was circumvented by placing the Al on top of the Ag which prevented it from contacting the crucible itself.

The graphite crucible was cleaned prior to use by vacuum firing at 1500 °C. Then Ag and Al in the desired ratio were heated above the melting point to form an alloy slug of 4–10 g. These slugs were cast into pellets 1.5 mm diam and 7 mm long, a size convenient for evaporation from a small filament. Filaments 3 cm long were made from 0.38-mm-diam tungsten wire. Two sample pellets were placed in a loop in the filament, which was then compressed to secure the pellets. Sample pellets were wetted to filaments in the demountable vacuum system before being mounted in the reflectometer.

The sample pellet size and location within the reflectometer was such that sizable amounts of sample remained on the filaments after deposition of films with thicknesses up to 10^4 Å. Complete evaporations were avoided to reduce contamination from material less volatile than the sample.

The substrates onto which the sample was evaporated were cut from optically polished quartz plate. Surfaces were cleaned with acetone and alcohol. As a test for cleanliness, each substrate surface was visually examined for uniform condensation of water vapor. Further cleaning was accomplished after a substrate was mounted in the

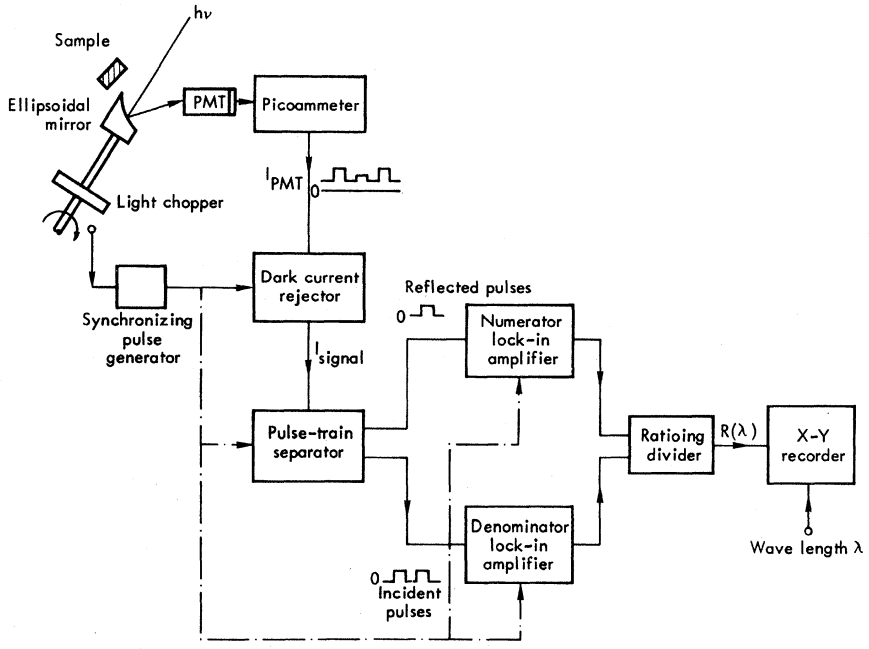

FIG. 3. Electronic-system block diagram for reflectance-ratio measurement.

reflectometer by heating the substrate to about 390 °C for 12 h while the ambient pressure was 10^{-7} Torr.

The two additional substrates, one on each side of the main substrate, served to collect an additional quantity of evaporated alloy sample. The additional film sample improved the accuracy of chemical analysis performed on the films after reflectance measurements were completed. Atomic absorption techniques were employed in making the final chemical analysis which was used to determine the alloy composition and to check for impurities. In particular, no evidence of carbon from the graphite crucible was detected in the final film.

Before evaporation, each sample was outgassed at successively higher temperatures while peak pressure was maintained in the low 10^{-8}-Torr range. When some deposition could be seen, current through the filament was increased to achieve a deposition rate in the range 30–90 Å/sec. Films thus produced had highly specular and uniform reflectance.

Films were annealed for 10–14 h at temperatures near 320 °C. Maximum pressure during annealing was usually less than 10^{-8} Torr.

C. Reflectance Measurements

A McPherson Model No. 225 monochromator with a hydrogen-discharge lamp was used for measurements in the range $3.9 < \hbar\omega < 11.6$ eV. A fused quartz filter with a cutoff at 7 eV was used to eliminate second-order light while reflectance measurements were being made at energies below 6.3 eV.

A Bausch and Lomb monochromator was used in the range $1.1 < \hbar\omega < 5.6$ eV. Deuterium and tungsten lamps provided high-intensity light for $3.1 < \hbar\omega < 5.6$ eV and $1.1 < \hbar\omega < 3.2$ eV, respectively. Appropriate filters were used to eliminate second-order light.

The reflectance over different spectral regions, measured with different light sources and monochromators, was fed into a computer. The data were then combined and replotted on a logarithmic scale by the computer. Figure 4 presents the results of reflectance measurements. Reflectance

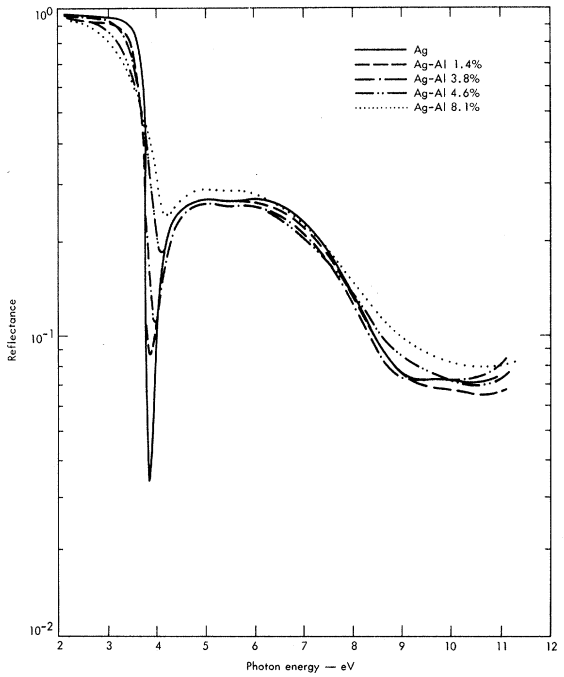

FIG. 4. Comparison of Ag and Ag-Al reflectances at 300 °K.

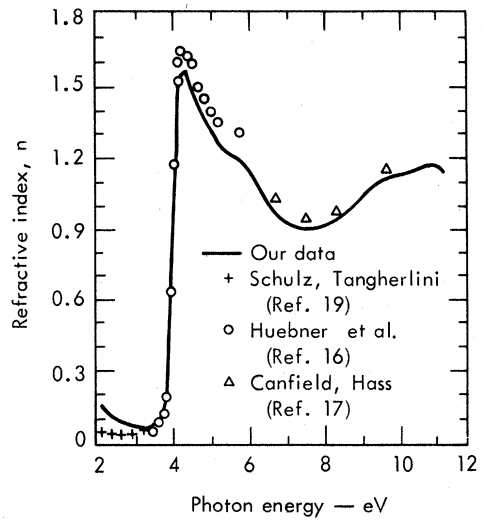

FIG. 5. Refractive index n for Ag.

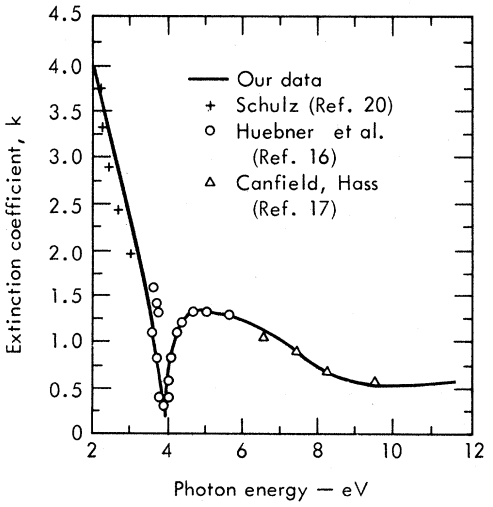

FIG. 6. Extinction coefficient k for Ag.

data are not presented for $\hbar\omega < 2$ eV. The data for that region are not sufficiently accurate because of the decreasing response with increasing wavelength of the *S*-11 photocathode used in the photomultiplier tube.

The high quality of the Ag film is indicated by the absence of the surface plasmon absorption peak that shows up at 3.65 eV in samples with rough surfaces.[6–9] Stanford[9] measured decreases in reflectance as much as 30% for samples with an rms surface roughness of 24 Å. Before the samples reported on here were annealed, the surface plasmon absorption was always observed, and a reflectance decrease of about 5% was noted. The absence of surface plasmon absorption after annealing suggests an rms surface roughness of less than a few Å.

III. DATA ANALYSIS

The optical constants n and k were determined from a Kramers-Kronig analysis of reflectance data. The method requires an integration over the entire spectrum to determine the phase change on reflectance. Thus, extrapolations are required for spectral regions outside the range of experimental data. For Ag and Ag-Al alloys, the reflectance approaches 1.0 as $\hbar\omega \to 0$, and a linear extrapolation between the measured reflectance at $\hbar\omega = 2$ eV and the theoretical reflectance of unity at $\hbar\omega = 0$ is quite satisfactory. The experimental data of other workers were used for reflectance in the range $11 < \hbar\omega < 40$ eV.[10,11] Above 40 eV, the empirical power law

$$R(\omega) = R_0(\omega/\omega_0)^{-2.02} \tag{1}$$

was used. R_0 is the reflectance at $\hbar\omega = 40$ eV, and ω_0 is the corresponding angular frequency.

The spectral dependence of n and k for pure silver is shown in Figs. 5 and 6. Also shown in the figures are values of n and k reported by other investigators.[12–15] In each case, the sample was an evaporated film measured at room temperature. The present studies differ in that the films were annealed. Other differences are the experimental method used and sample environment. Optical constants, shown in Figs. 5 and 6, that were reported by other investigators were determined by ellipsometry or multiple-angle reflectances, but not by use of the dispersion relation and normal incidence reflectance. Also, their samples were exposed to pressures of 10^{-6} Torr or higher. In view of these differences, agreement between their values and ours is good.

Using the n and k values obtained from an analysis of reflectance data, a number of optical functions of more direct physical interest were calculated. These are shown graphically in Figs. 7–10.

The real part of the dielectric function, ϵ_1, can be separated into free and bound parts ϵ_1^f and ϵ_1^b, respectively. The technique used is that employed by Ehrenreich and Philipp.[10] It depends upon the fact that the imaginary part of the dielectric function, ϵ_2, can also be separated into free and bound parts, and that these parts lie in separate spectral regions. Thus, ϵ_1^f and ϵ_1^b can be determined from a Kramers-Kronig analysis of ϵ_2^f and ϵ_2^b, respectively. The results for ϵ_1^b are shown in Fig. 7.

IV. DISCUSSION

Interband transitions in Ag begin at about 4 eV. As a result, below 2.5 eV, ϵ_1 is largely representative of ϵ_1^f. Figure 7 shows a peak in the ϵ_1 curves for Ag and the Ag-Al alloys near 4 eV. This peak is the contribution to ϵ_1 of ϵ_1^b, which is shown separately in the insert. Increasing solute concentration damps and broadens the peak in ϵ_1^b; it also moves to slightly higher energy the peak in ϵ_1 and the energy at which ϵ_1 first crosses zero. The latter is an indication of the shift in plasma frequency. The plasma frequency, and its shift to higher energy with increasing solute concentration, is defined more clearly by the peak in the electron loss function,

$$-\mathrm{Im}(1/\epsilon) = \epsilon_2/(\epsilon_1^2 + \epsilon_2^2), \tag{2}$$

shown in Fig. 10. These shifts are in the direction to be expected because of the increased electron

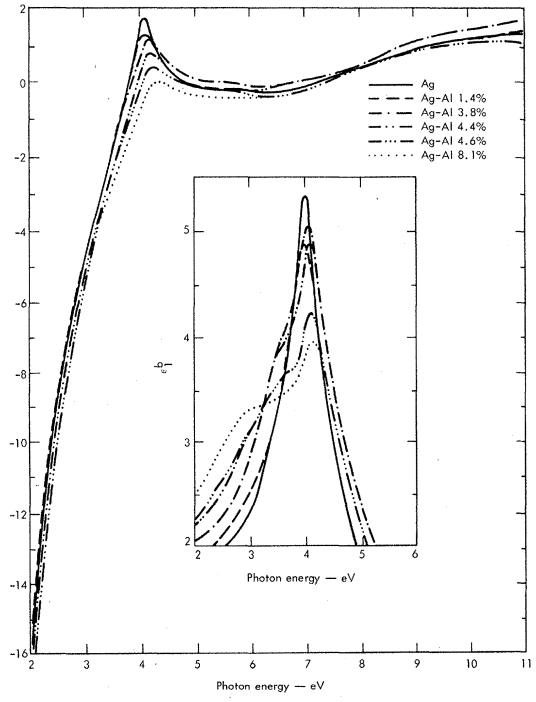

FIG. 7. ϵ_1 and ϵ_1^b vs photon energy for Ag and Ag-Al at 300°K.

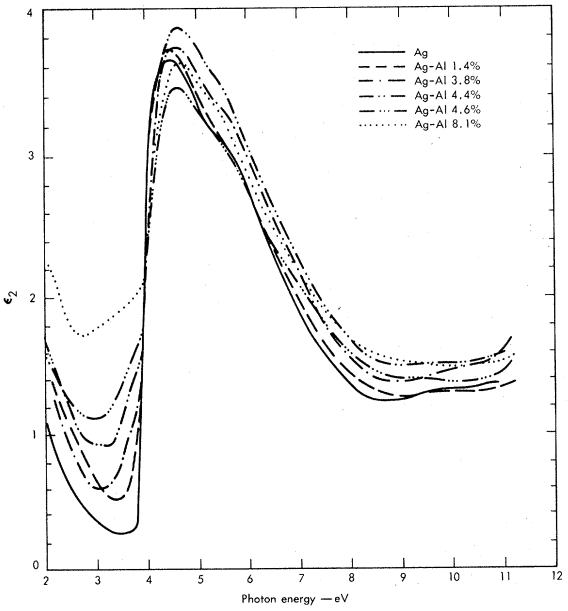

FIG. 8. ϵ_2 vs photon energy for Ag and Ag-Al at 300 °K.

concentration obtained on substituting Al for Ag. They also agree with measurements of electron characteristic energy-loss spectra.[16]

The main peak in ϵ_1^b near 4 eV shifts slowly to higher energy as Al is added to Ag. This peak is associated with the sharp rise in ϵ_2 (Figures 8 and

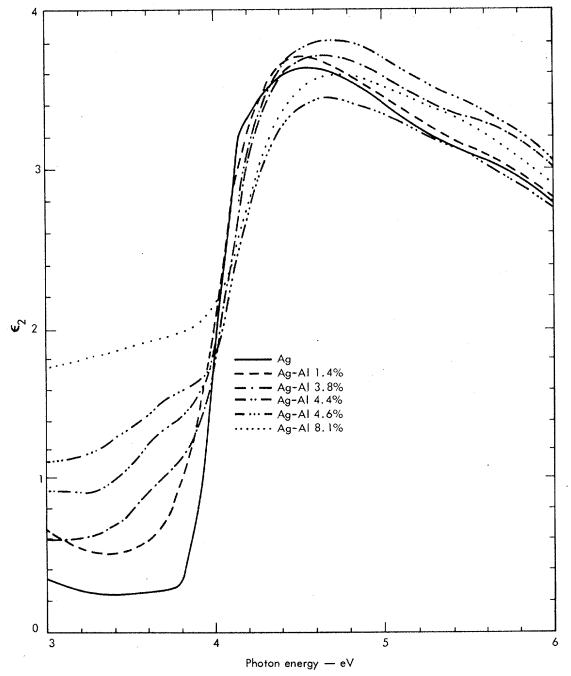

FIG. 9. ϵ_2 vs photon energy for Ag and Ag-Al at 300 °K.

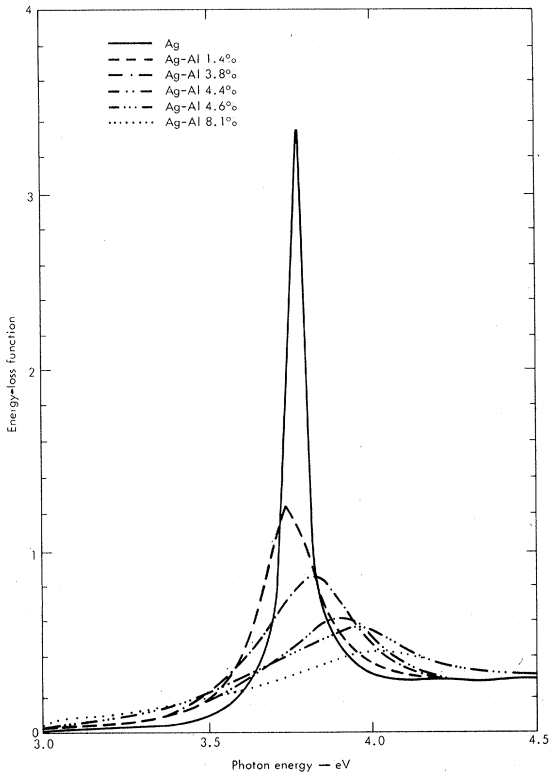

FIG. 10. Energy-loss function vs photon energy for Ag and Ag-Al at 300 °K.

9) at 3.9 eV and is identified with transitions from d states to the Fermi surface near L_3-$L_{2'}$.[6,13] A second structure emerges from ϵ_1^b and moves more quickly to lower energy with increasing Al concentration. The corresponding increase in ϵ_2 is shown in Figs. 8 and 9. The same effect has been reported in Ag-Cd and Ag-Zn alloys by Green[17] and in Ag-In alloys by Morgan and Lynch.[18] It is identified with interband transitions from the Fermi surface near $L_{2'}$ to a higher-lying conduction band near L_1. The rapid shift of the $L_{2'} \rightarrow L_1$ transition to lower energy is a result of the great sensitivity of the L_1 level to crystal potential.[19-21] The transition with an ϵ_2 peak at 5.73 eV is not shifted by alloying.

The shift in the $L_3 \rightarrow L_{2'}$ peak with Al concentration is shown in Fig. 11. Horizontal error bars show the estimated uncertainty in Al concentration; vertical error bars show the uncertainty in determining peak positions of ϵ_2 in the original calculations. The shift in energy expected on the basis of the rigid-band model is given by

$$\Delta E = (Z-1)n_a C/\rho(E_F), \tag{3}$$

where Z is the valence of the solute (3 for Al), n_a is the number density of atoms, C is the solute (Al) concentration, and $\rho(E_F)$ is the density of states

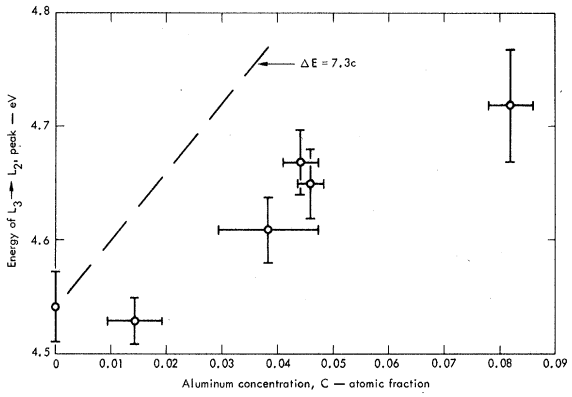

FIG. 11. Energy of $L_3 \rightarrow L_{2'}$ peak in Ag vs Al concentration C.

at the Fermi surface as obtained from heat-capacity measurements.[22] For Al, $\Delta E = 7.3\ C$ eV. This rate is about twice the rate observed. Since band calculations show the d band to be rather insensitive to the small changes in lattice potential expected in dilute alloys, it appears that one of the two extra valence electrons of Al remains fairly localized at the solute site. Thus, neither the rigid-band model, which predicts a change in Fermi energy given by Eq. (3), nor the Friedel model of localized states, which predicts no change in Fermi level, agrees with the experimental results. However, it is possible that part, if not all, of the shift in the L_3-$L_{2'}$ peak arises from smearing of the d-band edge by increased lifetime broadening. Then the d bands could be stationary in agreement with Friedel's theory. Also, since specific-heat measurements overestimate $\rho(E_F)$, the shift in energy calculated from Eq. (3) should perhaps be larger. This would further increase the discrepancy with the rigid-band model.

Stern[4] has recently shown that alloys of noble metals have unique electronic properties because of the large separation between the highest filled bands and the higher unoccupied bands. In particular, for polyvalent impurities such as Al, the shielding charge is necessarily spread out farther than calculated on the basis of free-electron shielding in the Thomas-Fermi model. As Stern shows, this follows from the theorem that in a completely filled band there are exactly two electrons around every atom for both the impurity and the host atoms. The present results suggest that the true description lies somewhere between the Friedel and the Stern theories.

---

*Work performed under the auspices of the U. S. Atomic Energy Commission.

†Fannie and John Hertz Foundation Fellow.

[1]N. F. Mott and H. Jones, *The Theory of the Properties of Metals and Alloys* (Dover, New York, 1958), pp. 170–174.

[2]J. Friedel, Advan. Phys. 3, 446 (1954).

[3]E. A. Stern, Phys. Rev. 157, 544 (1967).

[4]E. A. Stern, Phys. Rev. 188, 1163 (1969).

[5]T. Huen, G. B. Irani, and F. Wooten, Appl. Opt. (to be published).

[6]S. N. Jasperson and S. E. Schnatterly, Bull. Am. Phys. Soc. 12, 399 (1967).

[7]J. L. Stanford, H. E. Bennett, J. M. Bennett, E. J. Ashley, and E. T. Arakawa, Bull. Am. Phys. Soc. 13, 989 (1968).

[8]O. Hunderi and D. Beaglehole, Bull. Am. Phys. Soc. 14, 26 (1969).

[9]J. L. Stanford, J. Opt. Soc. Am. 60, 49 (1970).

[10]H. Ehrenreich and H. R. Philipp, Phys. Rev. 128, 1622 (1962).

[11]S. Robin, in *Optical Properties and Electronic Structure of Metals and Alloys*, edited by F. Abeles (North-Holland, Amsterdam, 1966), p. 202.

[12]L. G. Schulz, J. Opt. Soc. Am. 44, 357 (1954).

[13]L. G. Schulz and F. R. Tangherlini, J. Opt. Soc. Am. 44, 362 (1954).

[14]R. H. Huebner, E. T. Arakawa, R. A. MacRae, and R. N. Hamm, J. Opt. Soc. Am. 54, 1434 (1964).

[15]L. R. Canfield and G. Hass, J. Opt. Soc. Am. 55, 61 (1965).

[16]F. Fujimoto and O. Sueoka, J. Phys. Soc. Japan 19, 2069 (1964).

[17]E. L. Green, Phys. Rev. (to be published).

[18]R. M. Morgan and D. W. Lynch, Phys. Rev. 172, 628 (1968).

[19]C. E. Morris and D. W. Lynch, Phys. Rev. 182, 719 (1969).

[20]F. Herman and S. Skillman, in *Proceedings of the International Conference on Semiconductors, Prague*, 1960, edited by J. Bardeen (Czechoslovakian Academy of Sciences, Prague, 1961), p. 20.

[21]J. C. Phillips, Phys. Rev. 125, 1931 (1962).

[22]L. L. Isaacs, J. Chem. Phys. 43, 307 (1965).